

Electromagnetic Communication Laboratory Report No. 86-4

TIME-DOMAIN REFLECTOMETRY USING SCATTERING  
PARAMETERS AND A DE-EMBEDDING APPLICATION

by

A. S. Ali and R. Mittra

Technical Report

May 1986

Supported by

Office of Naval Research  
Contract No. N00014-85-K-0619

Electromagnetic Communication Laboratory  
Department of Electrical & Computer Engineering  
Engineering Experiment Station  
University of Illinois at Urbana-Champaign  
Urbana, Illinois 61801

"Reproduction in whole or in part is permitted for any purpose of the United States Government."

## TABLE OF CONTENTS

CHAPTER	PAGE
1. INTRODUCTION .....	1
1.1 Basic Time-domain Reflectometry .....	3
1.2 Scattering Parameters .....	7
1.3 Signal Flow When Measuring S-parameters .....	13
2. SYSTEMATIC MEASUREMENT ERRORS .....	17
2.1 Directivity Error .....	17
2.2 Source Match Error .....	19
2.3 Load Match Error .....	19
2.4 Isolation Error .....	19
2.5 Tracking Error .....	20
2.6 Error Correction and Calibration .....	20
2.6.1 Error Model and Analysis .....	20
2.6.2 Error Calibration .....	21
3. S-PARAMETER TDR DEVELOPMENT .....	23
3.1 Time-domain Analysis .....	23
3.2 Frequency-domain Analysis .....	28
4. IMPLEMENTATION AND PERFORMANCE OF THE S-PARAMETER TDR .....	29
4.1 System Rise Time .....	29
4.2 Frequency Range of Equipment .....	30
4.3 Processing Speed .....	31
4.4 S-parameter TDR Performance .....	32
4.5 Advantages of the S-parameter TDR .....	37
5. THE DE-EMBEDDING PROBLEM AND SOLUTION .....	41
6. CONCLUSIONS AND FUTURE WORK .....	48
LIST OF REFERENCES .....	49



Accession For	
NTIS CRA&I	<input checked="" type="checkbox"/>
DTIC TAB	<input type="checkbox"/>
Unannounced	<input type="checkbox"/>
Justification	
By .....	
Distribution /	
Availability Codes	
Dist	Avail and/or Special
A-1	

## CHAPTER I

### INTRODUCTION

With the advent of high-speed circuits and greater demands for wider bandwidths, devices and networks are being built to operate at super-high frequencies (tens of gigahertz). As frequencies get higher, perturbations caused by small discontinuities become more significant. When designing high-frequency devices, engineers routinely wish to examine their characteristics and compensate for unwanted perturbations. This is done most often using time-domain reflectometry (TDR) techniques [1]. In using a TDR technique, the reflected signal provides important information about the device under test (DUT). It also contains information about any intervening connections between the DUT and the measuring or test set. This "connector" information is considered to be a distortion since the engineer wishes to observe the DUT alone, and not the DUT/connector composite. Many researchers have investigated techniques which can be utilized in solving the problem of removing this "connector" distortion. A brief discussion of some of their works is provided below.

Farber and Ho [2] developed a time-domain system to measure frequency-domain driving points and transfer impedances of DUTs. In their work, they developed a time-to-frequency transformation (TFT) by using an on-line computer and a sampling oscilloscope. They then applied a fast Fourier transform (FFT) algorithm to process reflections from the DUT when the excitation source was a known pulse. Their technique provided good accuracy up to one gigahertz. Although they did not apply their TFT specifically

to the distortion removal problem, they demonstrated a viable approach to time-domain simulations.

Later, Nicolson et al. [3] developed a similar measurement technique, which they used to obtain frequency-domain data of networks by sampling time-domain transient responses. Bauer and Penfield [4] examined the de-embedding problem and presented the well-known formula for de-embedding. In their study, they employed the classical z-parameters. Scattering or s-parameters were utilized by Loeb and Ward [5]. After extracting time-domain data, they shifted the measurement plane to de-embed the unwanted reflections.

This thesis examines the de-embedding problem from a point of view similar to that of Loeb and Ward and proposes a modern technique which directly utilizes s-parameters. The objective of acquiring measured data that represent the DUT alone will be accomplished by first developing a TDR technique using scattering parameters and then processing the inverted time-domain data to remove the effects of any intervening connections between the DUT and the measuring set.

To satisfy the above objective, the thesis follows the sequence of first examining basic TDR systems and establishing what needs to be simulated. Second, s-parameters and errors inherent in measuring them are reviewed. Error analysis and error models are then developed. With appropriate error models, the actual TDR technique using s-parameters is developed and application to the specific problem is presented. Advantages of this technique are also discussed.

## 1.1 Basic Time-domain Reflectometry

Time-Domain Reflectometry (TDR) is a measurement technique which is widely used. Two of its primary uses include finding the distance to a discontinuity along a transmission line and determining the impedance of a network or DUT. The latter is feasible because the amplitude of the reflected signal corresponds directly to the impedance of the DUT.

A generalized reflectometer consists of a sweeping source, a signal separation device, a detector, a DUT, some standard loads to use as references, and usually a display device as shown in Figure 1. In network analysis, the reflection coefficient of the DUT is of prime importance. In this case, the source sends a signal at each frequency of interest and the ratio of the reflected signal to the incident signal is measured. The incident signal is sampled from the forward port of the signal separation device or directional coupler, while the reflected signal is sampled from the reverse port of the coupler.

If there were no requirement for spectrum analysis and only network analysis was required, then an even more basic time-domain reflectometer could be used. In this case, it would consist of a high-frequency oscilloscope, a high-frequency pulse generator, a reference transmission line, appropriate standard terminations, and a DUT, as shown in Figure 2. Here the generator sends a pulse towards the DUT and the scope measures and displays the sum of the incident and reflected signals. When the reference transmission line is terminated with a true open circuit, the reflection coefficient has unit magnitude and zero phase. The reflected and incident signals add constructively and result in the waveform shown in Figure 3(a). When it is terminated with a

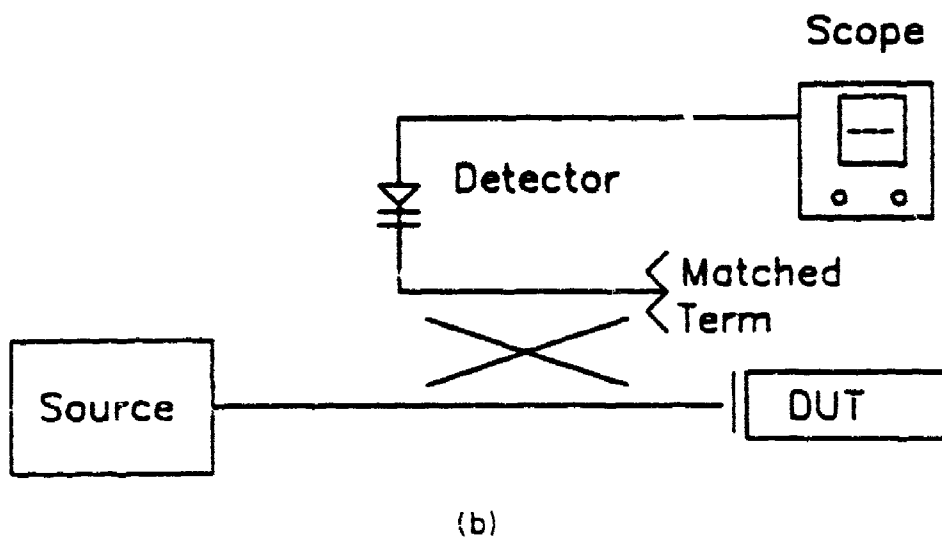
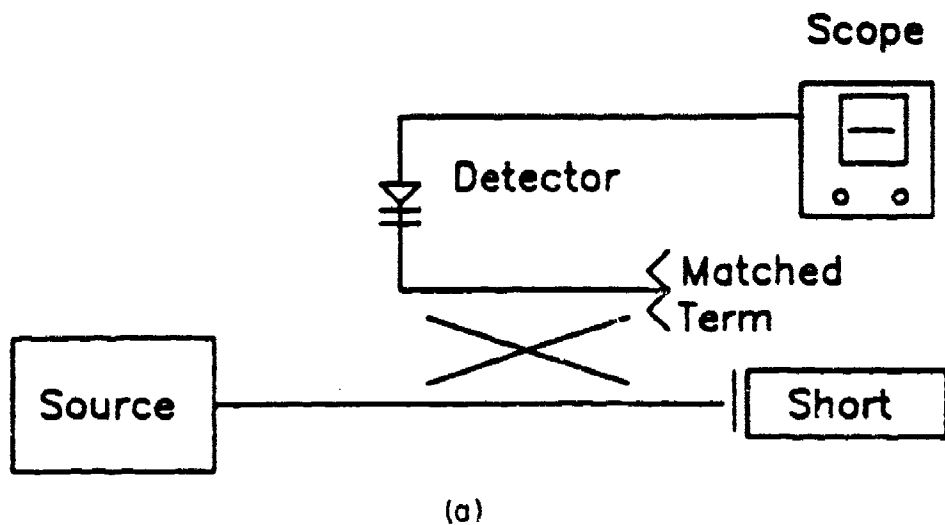


Figure 1. Generalized Reflectometer. (a) Establishing a Reference for the Reflection Coefficient with Short-circuit Termination. (b) Measuring the Reflection Coefficient of the DUT.

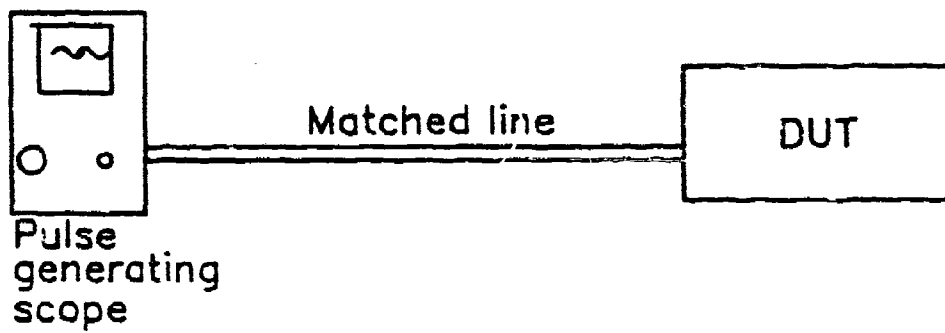


Figure 2. Basic Time-domain Reflectometer Utilizing an Oscilloscope, a Pulse Generator, and a Reference Transmission Line.

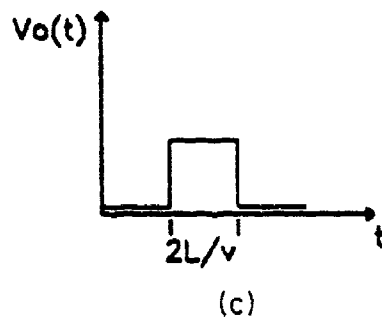
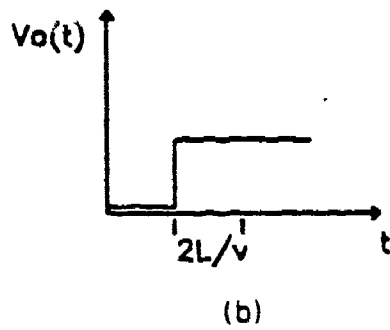
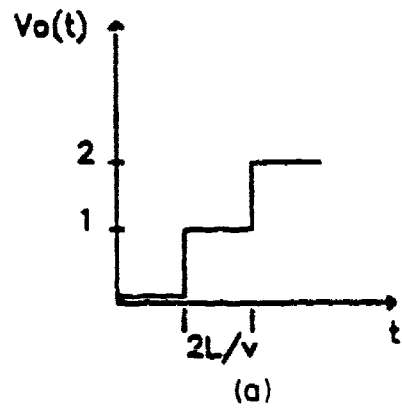


Figure 3. Idealized Waveforms for Different Terminations. (a) Open Circuit (b) Matched 50-ohm Load and (c) Short Circuit.

true short, the reflection coefficient has unit magnitude and a 180 degree phase. The incident and reflected signals add destructively and produce the waveform of Figure 3(b). For a truly matched termination, the reflection coefficient has zero magnitude and the waveform of Figure 3(c) is generated.

The above waveforms cannot be realized in practice because of the lead inductances and capacitances. These capacitive and inductive effects are indicated in Figure 4. The higher the frequency, the more significant the fringing effects of the electric field of open terminations. Similar distortions occur for the short and matched terminations. More importantly though, at these higher frequencies, systematic measurement errors manifest themselves in a more pronounced manner. These undesirable effects can be reduced significantly by using scattering parameters and appropriate error correction techniques. Using these techniques, *s*-parameters will be measured and used to simulate the time-domain response of a DUT which is subjected to a pulse of appropriate pulse width. The strategy then is to begin by introducing *s*-parameters and error correction.

## 1.2 Scattering Parameters

Any two-port network, such as that shown in Figure 5, can be characterized by a number of familiar parameters. It can, for example, be described by its hybrid (*h*), impedance (*z*), or admittance (*y*) parameters as follows:

*h*-parameters

$$V_1 = h_{11}I_1 + h_{12}V_2$$

$$I_2 = h_{21}I_1 + h_{22}V_2$$

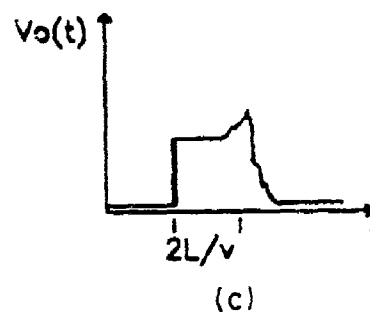
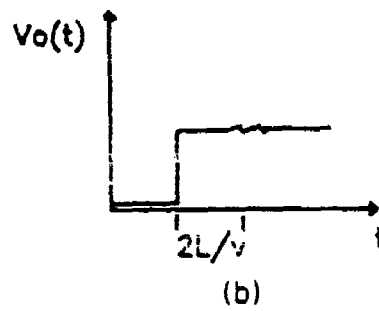
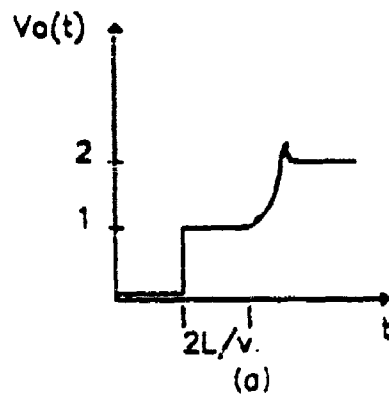


Figure 4. Realistic Waveforms Demonstrating the Fringing Effects of the Electric Field. (a) Open-circuit Termination, (b) Matched 50-ohm Termination, and (c) Short-circuit Termination.

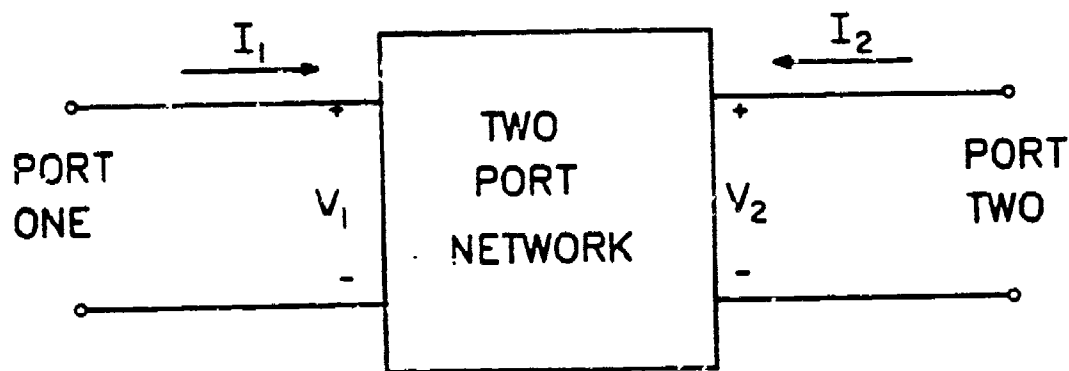


Figure 5. Generalized Two-port Network.

y-parameters

$$I_1 = y_{11}V_1 + y_{12}V_2$$

$$I_2 = y_{21}V_1 + y_{22}V_2$$

z-parameters

$$V_1 = z_{11}I_1 + z_{12}I_2$$

$$V_2 = z_{21}I_1 + z_{22}I_2$$

While these familiar parameters are adequate for characterizing the two port at low frequencies, they are difficult to determine at high frequencies. The difficulty stems primarily from the requirement of realizing a true open and short termination. For example, to determine  $h_{11}$ , the ratio of  $V_1$  to  $I_1$  is needed when  $V_2=0$ . That is, port two must be terminated in a short cir-

cuit. If  $h_{12}$  is desired, the ratio  $V_1/V_2$  would be needed when  $I_1=0$ , i.e., open port one. Similarly, for  $y_{21}=I_2/V_1$ , port two must be short circuited.

Having to open or short circuit the terminals of a two-port network in order to determine its parameters is not an acceptable condition. Not only must the engineer be concerned with the difficulties encountered when trying to realize a true open or short termination at high frequencies, but also with the stability of the two port itself. Active devices, such as transistors and tunnel diodes, are often not short or open circuit stable; they may be driven into oscillation. Additionally, these low frequency parameters do not provide the most convenient physical insight into the two-port characteristics. These are some of the main reasons why s-parameters are used to characterize networks at high frequencies.

Given the two port as shown in Figure 6, K. Kurokawa and others defined the generalized scattering parameters [6][7]. These parameters describe the interrelationships between the complex voltage waves given below.

$$\begin{aligned}
 a_1 &= \frac{V_1 + I_1 Z_0}{2\sqrt{Z_0}} \\
 &= \frac{\text{Complex voltage wave incident on port 1}}{\sqrt{Z_0}} \\
 &= \frac{V_{11}}{\sqrt{Z_0}} \\
 a_2 &= \frac{V_2 + I_2 Z_0}{2\sqrt{Z_0}} \\
 &= \frac{\text{Complex voltage wave incident on port 2}}{\sqrt{Z_0}}
 \end{aligned}$$

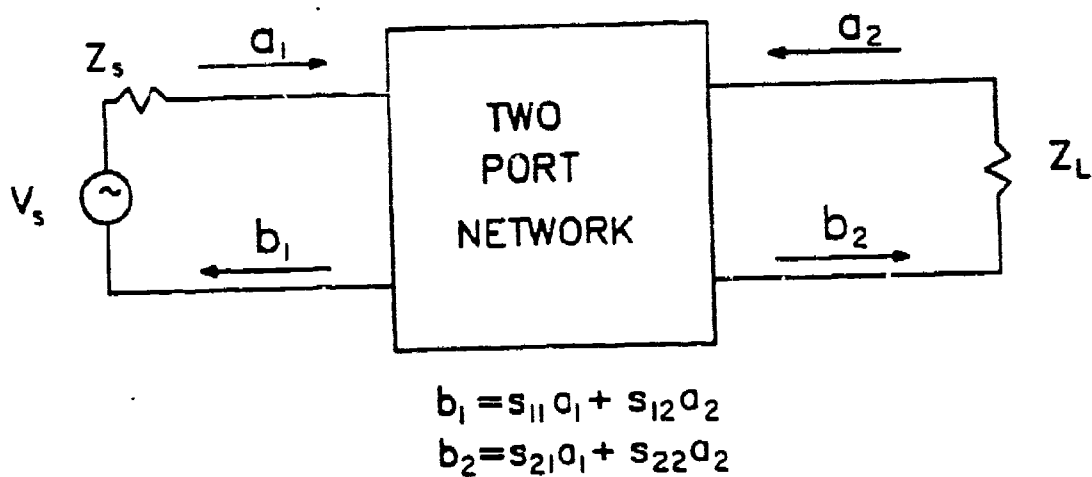


Figure 6. Two-port Network Showing Where the Voltage/Power Waves Are Defined.

$$a_1 = \frac{V_{i1}}{\sqrt{Z_{i1}}}$$

$$b_1 = \frac{V_1 - I_1 Z_{i1}}{2\sqrt{Z_{i1}}}$$

= Complex voltage wave reflected from port 1

$\sqrt{Z_{i1}}$

$$= \frac{V_{r1}}{\sqrt{Z_{i1}}}$$

$$b_2 = \frac{V_2 - I_2 Z_{o2}}{2\sqrt{Z_{o2}}}$$

= Complex voltage wave reflected from port 2

$\sqrt{Z_{o2}}$

$$b_2 = \frac{V_{r2}}{\sqrt{Z_0}}$$

With these voltage waves, the two-port network can be characterized in terms of s-parameters:

$$b_1 = s_{11}a_1 + s_{12}a_2$$

$$b_2 = s_{21}a_1 + s_{22}a_2$$

From the above characterizations, s-parameters can be determined and interpreted as below :

$$S_{11} = \left. \frac{b_1}{a_1} \right|_{a_2=0} \quad (Z_L = Z_0 \rightarrow a_2 = 0)$$

= Input reflection coefficient with output port terminated in a matched load.

$$S_{22} = \left. \frac{b_2}{a_2} \right|_{a_1=0} \quad (Z_s = Z_0 \text{ and } V_s = 0 \rightarrow a_1 = 0)$$

= Output reflection coefficient with input port terminated in a matched load.

$$S_{21} = \left. \frac{b_2}{a_1} \right|_{a_2=0} \quad (Z_L = Z_0 \rightarrow a_2 = 0)$$

= Forward transmission (insertion) gain with output port terminated in a matched load.

$$S_{12} = \left. \frac{b_1}{a_2} \right|_{a_1=0} \quad (Z_s = Z_0 \text{ and } V_s = 0 \rightarrow a_1 = 0)$$

= Reverse transmission coefficient with input port terminated in a matched load.

With the s-parameters determined as above, a better insight is available about the operation of the network from the following interpretations of the incident and reflected waves.

$$|a_1|^2 = \text{Power incident on input of network.}$$

= Power available from source of impedance  $Z_0$ .

$$|a_2|^2 = \text{Power incident on the output of the network.}$$

= Power reflected from the load.

$$|b_1|^2 = \text{Power reflected from the input of the network.}$$

= Power from a  $Z_0$  source minus the power delivered to the input of the network.

$$|b_2|^2 = \text{Power reflected from the output of the network.}$$

= Power incident on the load

= Power that would be delivered to a  $Z_0$  load.

Similarly, there is a better insight into the s-parameters:

$$|S_{11}|^2 = \frac{\text{Power reflected from input of network}}{\text{Power incident on the input of network}}$$

$$|S_{22}|^2 = \frac{\text{Power reflected from output of network}}{\text{Power incident on the output of network}}$$

$$|S_{21}|^2 = \frac{\text{Power delivered to a } Z_0 \text{ load}}{\text{Power available from a } Z_0 \text{ source}}$$

= Transducer power gain with a  $Z_0$  load and source.

$$|S_{12}|^2 = \text{Reverse transducer power gain with a } Z_0 \text{ load and source.}$$

### 1.3 Signal Flow When Measuring S-parameters

Figures 7 and 8 show the equipment layout used to measure s-parameters. A typical signal flow begins with the sweep oscillator. It must have the appropriate RF plug-in to cover the frequency range of interest. In this thesis, the range of interest was dc to 18 GHz. After the signal leaves the oscillator, it splits into two when inside the test set (Figure 8). One signal is

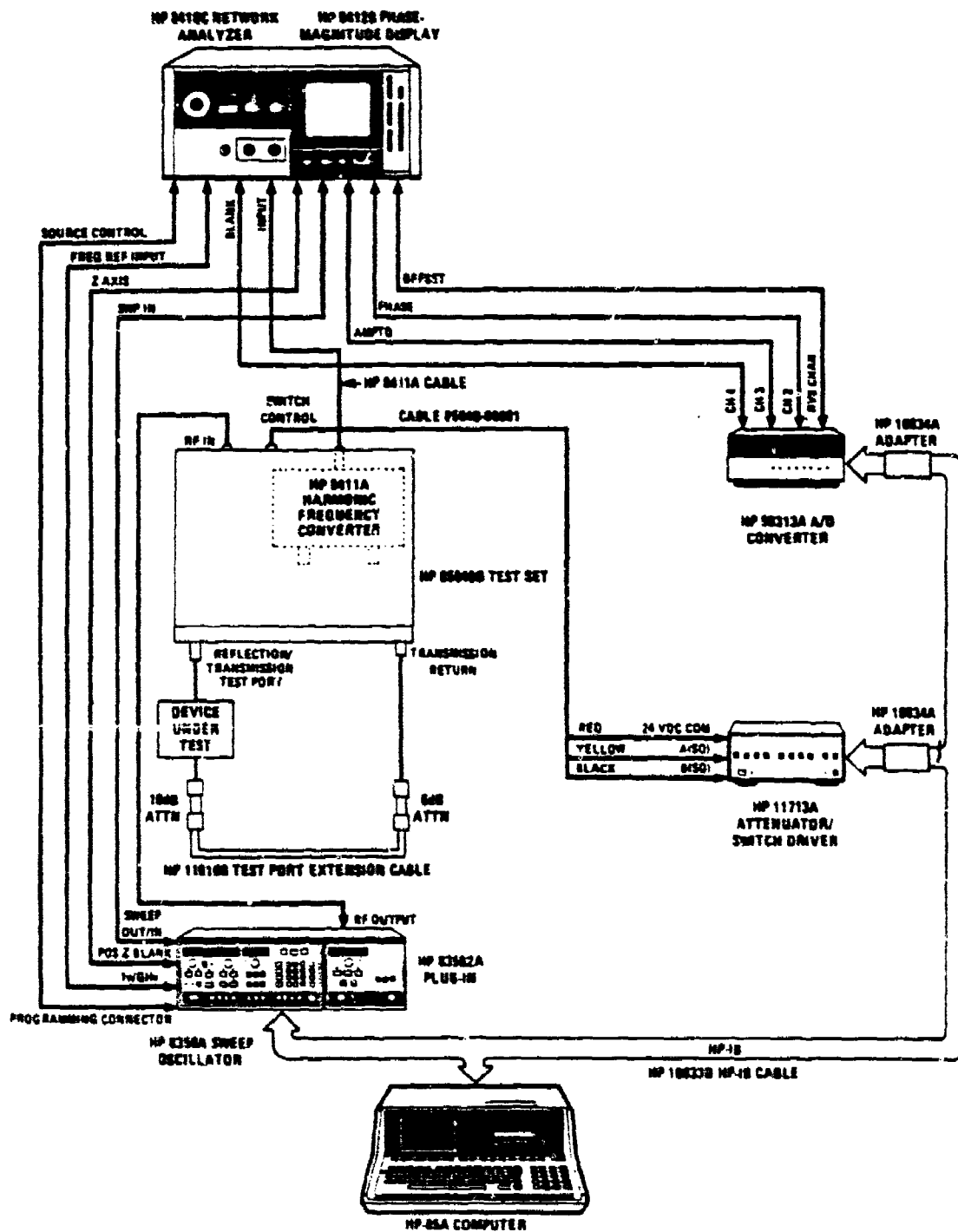


Figure 7. Signal Flow When Measuring S-parameters. Schematic Taken from Hewlett-Packard Manual for the 85040B Test Set, pp. 2-8, May 1982.

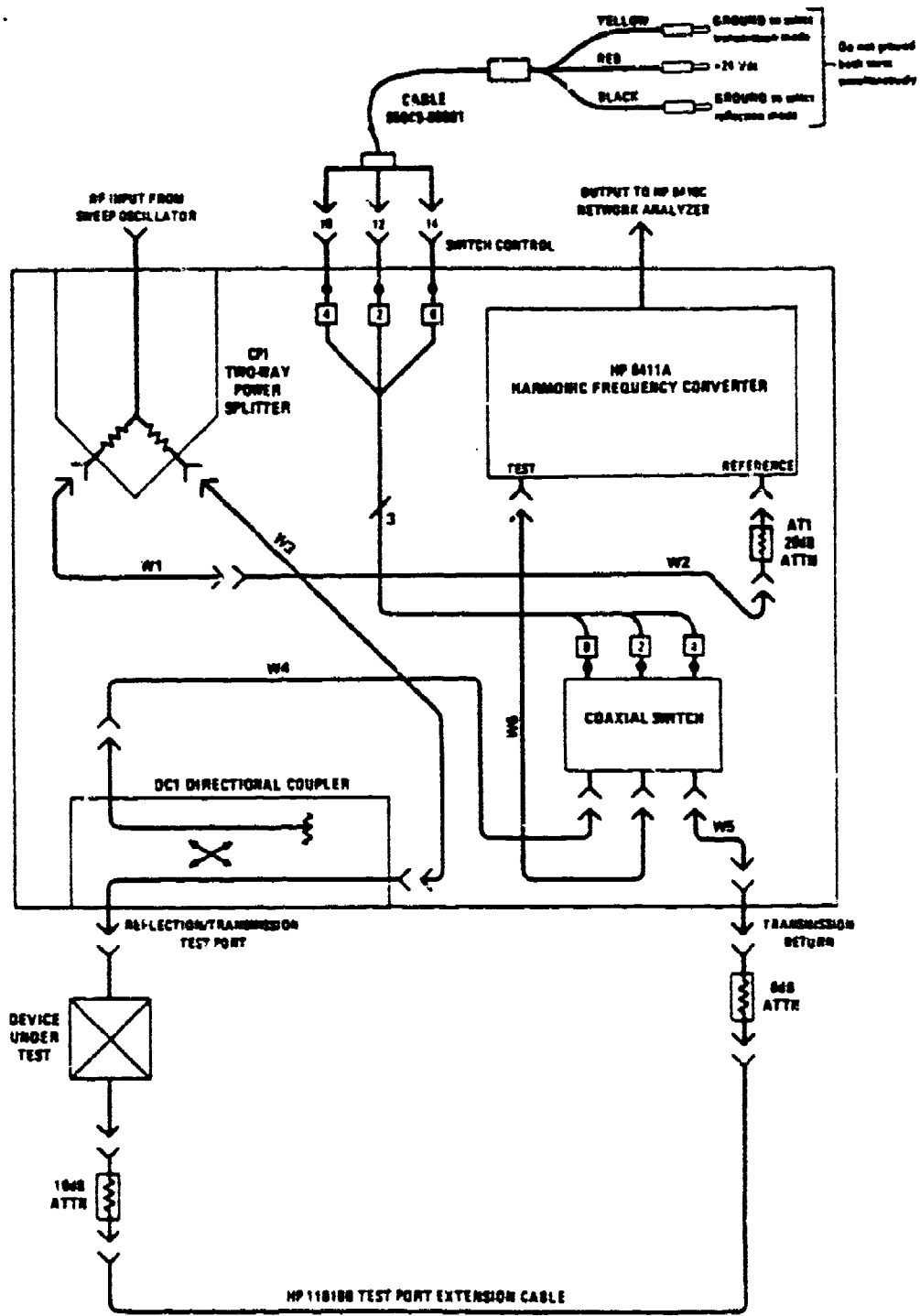


Figure 8. Block Diagram of Test Set Showing Signal Flow When Measuring S-parameters. Schematic Taken from Hewlett-Packard Manual for the 85040B Test Set, pp. 8-0, May 1982.

sampled directly by the reference port of the harmonic converter and used as a reference. The other is made incident on the DUT and will eventually be sampled by the test port of the harmonic converter.

When the interest is in measuring the transmission coefficient,  $S_{21}$ , port two of the DUT is connected to the Transmission/Return port of the test set. The controller (computer) then selects the transmission path via the coaxial switch, and the signal is routed to the test port of the harmonic converter. The reference and transmission signals are then down-converted by the harmonic converter to a constant 20.278 MHz intermediate frequency (IF) signal. Impressed on this IF signal are the relative phase and magnitude of the transmission signal compared to the reference signal. A similar sequence occurs when making reflection or  $S_{11}$  measurements. The reference and test signals are routed as before. This time, the controller selects the reflection path via the coaxial switch. The reflected signal is then sent to the harmonic converter which impresses on the IF signal the magnitude and phase information. The information from the harmonic converter is then sent to the network analyzer.

The network analyzer extracts the magnitude and phase information from the IF signal and sends it to the display unit. This unit displays the amplitude or phase information as a function of frequency and outputs analog voltages proportional to the magnitude and phase information. These analog signals are converted to digital format by the A/D converter that is polled by the controller. Once the controller receives the magnitude and phase information, processing begins. Specific processing is addressed later.

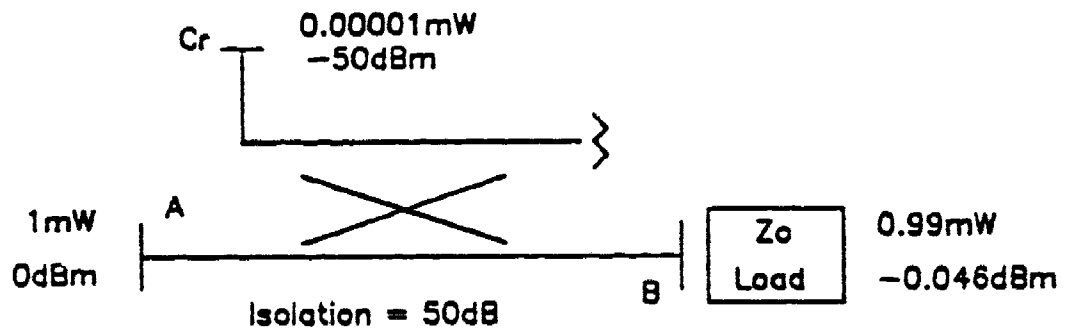
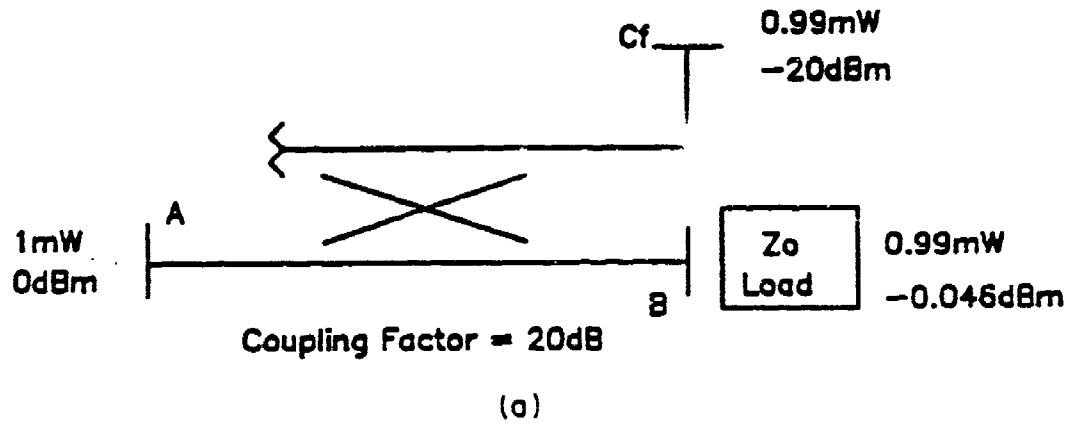
## CHAPTER 2

### SYSTEMATIC MEASUREMENT ERRORS

In tracing the signal flow as outlined above, points at which systematic measurement errors can potentially be interjected into the system can be identified [8]. One prime source of error is the directional coupler used in the test set. Ideally, this device absolutely separates the forward signal from the reverse signal. This never occurs in reality and directivity errors result. Another source of error is the signal generator. When the generator fails to maintain absolute constant power at the input of the DUT, or when its output impedance is not perfectly matched to the transmission line, source match errors are produced. A third contributor is the impedance mismatch between the output port of the DUT and the input port of the network analyzer. These mismatches result in load match errors. Occasionally, there is cross coupling between reference and test signals in the test set. This contributes to isolation errors. The final major systematic error is the tracking error which results from components such as cables and adapters, that have magnitude and phase responses which vary as a function of frequency. That is, their responses are not flat across the frequency band of interest.

#### 2.1 Directivity Error

Directivity is defined as the ratio of the power coupled into the coupled arm when the coupler is in the forward direction and using a  $Z_0$  load to the power available in the coupled arm when the coupler is in the reverse direction and using a  $Z_0$  load. Figure 9 shows the schematic of a coupler. It also



$$\text{Directivity} = 10 \log Cf/Cr = 30\text{dB}$$

(b)

Figure 9. Schematic of Directional Coupler Demonstrating How to Compute Directivity. (a) Signal Flow in the Forward Direction. (b) Signal Flow in the Reverse Direction.

demonstrates how to compute directivity, given an input signal of 1 mW and a detected signal of 0.99 mW when in the forward direction and a detected signal of 0.00001 mW when in the reverse direction.

The primary contributor of imperfect directivity is the leakage between the forward and reverse signal paths. There are also significant contributions from connector reflections and coupler load reflections.

## 2.2 Source Match Error

The source is in a levelling loop. It tries to maintain an absolute constant power at the input of the DUT. This is very difficult because there are cable and adapter mismatches and losses outside the levelling loop. The effect is that the reflection coefficient of the source as "seen" from the outside world is not zero, i.e.,  $\Gamma_s \neq 0$ . This means that the source cannot compensate quickly enough, and source match errors are produced.

## 2.3 Load Match Error

During transmission measurements, the signal may encounter many discontinuities caused by impedance mismatches as it travels from the output port of the DUT to the input port of the network analyzer. The vector sum of all these error signals contributes to load match errors.

## 2.4 Isolation Error

Occasionally, there is leakage between IF and RF signals in the receiver section of the network analyzer. Both leakage and cross coupling, which occur between reference and test signals to the harmonic converter,

contribute to isolation error.

## 2.5 Tracking Error

Different test setups using different connectors, cables, adapters, etc. with different magnitudes and phase responses contribute to tracking error. Tracking error depends primarily on the lengths of cables used.

## 2.6 Error Correction and Calibration

Now that the major sources of errors have been identified, an appropriate error model is developed in order to calibrate the measurement system and neutralize these errors. Since the prime interest is in developing a TDR technique for a one-port device, the error analysis is restricted to a three-term error model.

### 2.6.1 Error Model and Analysis

Figure 10 shows the three-term error model. Of primary interest is the reflection coefficient  $S_{11}$ . Since the reflected signal  $R$  is invariably corrupted by leakage through the directional coupler, the directivity error  $E_{dl}$  is modeled by a forward path from incident to reflected signal. For signals that are reflected from the DUT and get rereflected from mismatches, the source match error  $E_{sr}$  is modeled as a path from reflected to incident signal. Since test signals travel different paths than reference signals, they are distorted by intervening hardware which have variations in their magnitude and phase flatness. These different paths contribute to tracking error  $E_{tr}$  which is modeled along the reflected signal path.

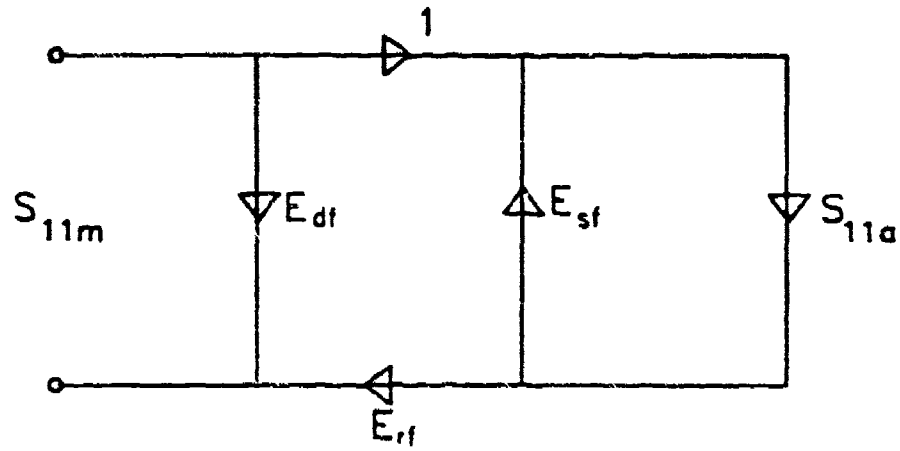


Figure 10. Three-term Error Model.

Figure 10 shows that there are only two independent paths,  $E_{df}$  and  $S_{11a}E_{rf}$ , between the incident and reflected signals. There is also only one closed loop,  $S_{11a}E_{rf}$ . By applying Mason's rule [9][10], the measured input reflection coefficient  $S_{11m}$  is

$$S_{11m} = E_{df} + \frac{S_{11a}E_{rf}}{1 - E_{rf}S_{11a}} \quad (2.6.1)$$

### 2.6.2 Error Calibration

Equation (2.6.1) has four unknowns:  $E_{df}$ ,  $E_{rf}$ ,  $E_{sf}$ , and  $S_{11a}$ . The  $S_{11m}$  term is a measured quantity. Using three standard terminations, i.e., terminations which have known values of  $S_{11}$ , the other three unknowns,  $E_{df}$ ,  $E_{rf}$ , and  $E_{sf}$ ,

can be determined. The three standards and their corresponding  $S_{11,m}$  are (1) Open termination,  $S_{11,m} = 1$ ; (2) Short termination,  $S_{11,m} = -1$ ; and (3) Matched load,  $S_{11,m} = 0$ . Taking three measurements of  $S_{11,m}$  produces three equations in the three unknowns. These equations can then be solved to obtain the three error terms. Equation (2.6.1) can be rewritten in terms of  $S_{11,m}$  as

$$S_{11,a} = \frac{S_{11,m} - E_{df}}{E_{rf}(S_{11,m} - E_{df}) + E_{rf}} \quad (2.6.2)$$

After determining the three error terms,  $E_{df}$ ,  $E_{rf}$ , and  $E_{tt}$ , Eq. (2.6.2) can be used to process any measured  $S_{11,m}$  of the DUT and obtain its actual  $S_{11,a}$ .

## CHAPTER 3

### S-PARAMETER TDR DEVELOPMENT

Equipped with some understanding of s-parameters and error modeling, a TDR using s-parameters is developed. To get some physical insight, a time-domain analysis is first performed on the transmission line system shown in Figure 11. It is then shown that this method supports the s-parameter solution derived later.

#### 3.1 Time-domain Analysis

To simulate the TDR, an expression must first be obtained for  $V_o(z,t)$  as shown in Figure 11. This means that the Maxwell's equations shown below have to be solved for the transmission line.

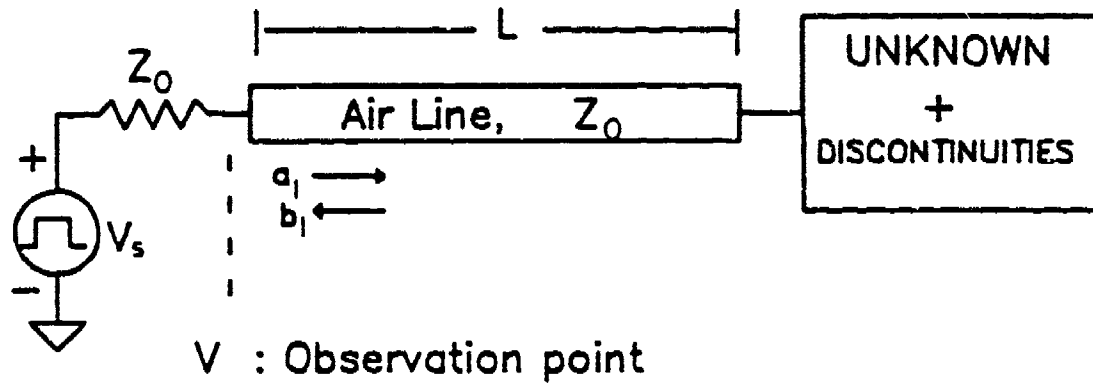
$$\frac{\partial V}{\partial z} = -L \frac{\partial I}{\partial t}$$
$$\frac{\partial I}{\partial z} = -GV - C \frac{\partial V}{\partial t}$$

The solutions for the voltage  $V_o$  and current  $I_o$  that satisfy Maxwell's equations can be written as positive and negative traveling waves of the form

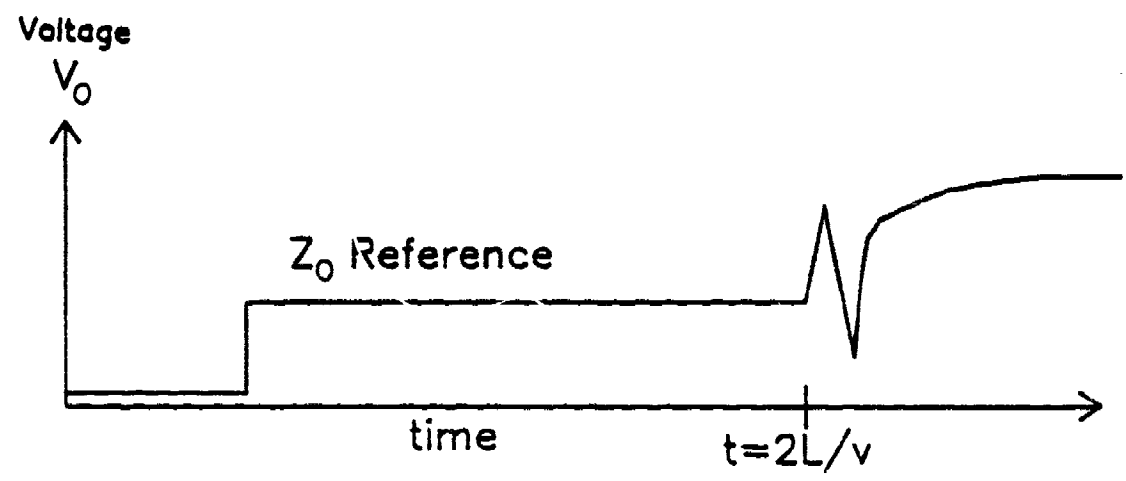
$$V_o(z) = Ae^{-jkz} + Be^{jkz} \quad (3.1.1)$$

$$I_o(z) = \frac{1}{Z_o} (Ae^{-jkz} - Be^{jkz}) \quad (3.1.2)$$

The boundary conditions to be satisfied are



(a)



(b)

Figure 11. Schematic of Measurement Setup Showing (a) Where the Voltage  $V_0(t)$  is Observed and (b) a Typical Response To Be Simulated.

$$V_o(0) = A + B = V_s - Z_s \frac{A - B}{Z_o} \quad (3.1.3)$$

$$V_o(l) = Ae^{-jkl} + Be^{jkl} = Z_L I_L = Z_L \frac{1}{Z_o} (Ae^{-jkl} - Be^{jkl}) \quad (3.1.4)$$

From Eq. (3.1.3)

$$A(1 + Z_s/Z_o) = -B(1 - Z_s/Z_o) + V_s$$

$$A = B \frac{(Z_s/Z_o - 1)}{(Z_s/Z_o + 1)} + \frac{V_s}{(Z_s/Z_o + 1)}$$

$$A = B \frac{Z_s - Z_o}{Z_s + Z_o} + V_s \frac{Z_o}{Z_s + Z_o}$$

$$A = B\Gamma_s + TV_s \quad (3.1.5)$$

where  $\Gamma_s$ ,  $T$ , and  $\Gamma_L$  were defined as

$$\Gamma_s = \frac{Z_s - Z_o}{Z_s + Z_o}$$

$$T = \frac{Z_o}{Z_s + Z_o}$$

and

$$\Gamma_L = \frac{Z_L - Z_o}{Z_L + Z_o}$$

From Eq. (3.1.4)

$$Ae^{-jkl}(1 - Z_L/Z_o) = -Be^{jkl}(1 + Z_L/Z_o)$$

$$B = Ae^{-j2kl} \frac{(Z_L/Z_o - 1)}{(Z_L/Z_o + 1)} = Ae^{-j2kl} \frac{(Z_L - Z_o)}{(Z_L + Z_o)}$$

$$B = \Gamma_L Ae^{-j2kl} \quad (3.1.6)$$

Substituting Eq. (3.1.6) into Eq. (3.1.5) results in

$$A = A\Gamma_1\Gamma_L e^{-j2kl} + TV_s \rightarrow A(1 - \Gamma_1\Gamma_L e^{-j2kl}) = TV_s$$

$$A = \frac{TV_s}{1 - \Gamma_1\Gamma_L e^{-j2kl}} \quad (3.1.7)$$

$$B = \frac{\Gamma_L TV_s e^{-j2kl}}{1 - \Gamma_1\Gamma_L e^{-j2kl}} \quad (3.1.8)$$

Recognizing that  $\Gamma_1\Gamma_L < 1$  and that  $\frac{1}{1-a} = \sum_{n=0}^{\infty} a^n$  if  $a < 1$ , A and B can be written as

$$A = TV_s \sum_{n=0}^{\infty} (\Gamma_1\Gamma_L)^n e^{-j2nkl} \quad (3.1.9)$$

and

$$B = TV_s \Gamma_L e^{-j2kl} \sum_{n=1}^{\infty} (\Gamma_1\Gamma_L)^{n-1} e^{-j2nkl} \quad (3.1.10)$$

From Eq. (3.1.1)

$$\begin{aligned} V_o(z) &= Ae^{-jkz} + Be^{jkz} = Ae^{-jkz} + A\Gamma_L e^{-j2kl} e^{jkz} \\ &= TV_s \sum_{n=0}^{\infty} (\Gamma_1\Gamma_L)^n e^{-j2nkl} [e^{-jkz} + \Gamma_L e^{-jk(2l-z)}] \\ V_o(z) &= \Gamma \sum_{n=1}^{\infty} (\Gamma_1\Gamma_L)^n V_s [e^{-jk(2nl+z)} + \Gamma_L e^{-jk(2nl+2l-z)}] \end{aligned} \quad (3.1.11)$$

Substituting  $k = \omega/v$  yields

$$V_o(z) = \Gamma \sum_{n=1}^{\infty} (\Gamma_1\Gamma_L)^n V_s [e^{-j\omega \frac{1}{v}(2nl+z)} + \Gamma_L e^{-j\omega \frac{1}{v}(2nl+2l-z)}] \quad (3.1.12)$$

The strategy now is to recognize Eq. (3.1.12) as the Fourier transform of

$V_s(t)$  shifted in the first term by  $\frac{1}{v}(2nl + z)$  and shifted and scaled in the second term by  $\frac{1}{v}(2nl + 2l - z)$  and  $\Gamma_L$  respectively, i.e.,

$$V_o(z,t) = T \sum_{n=0}^{\infty} (\Gamma, \Gamma_L)^n [V_s(t - \frac{1}{v}(2nl + z)) + \Gamma_L V_s(t - \frac{1}{v}(2nl + 2l - z))] \quad (3.1.13)$$

Expanding  $V_o(z,t)$ :

$$\begin{aligned} V_o(z,t) &= T [V_s(t - \frac{z}{v}) + \Gamma_L V_s(t - \frac{1}{v}(2l - z))] & (n=0) \\ &+ T \Gamma, \Gamma_L [V_s(t - \frac{1}{v}(2l + z)) + \Gamma_L V_s(t - \frac{1}{v}(4l - z))] & (n=1) \\ &+ T (\Gamma, \Gamma_L)^2 [V_s(t - \frac{1}{v}(4l + z)) + \Gamma_L V_s(t - \frac{1}{v}(6l - z))] & (n=2) \\ &+ T \sum_{n=3}^{\infty} (\Gamma, \Gamma_L)^n [V_s(t - \frac{1}{v}(2nl + z)) + \Gamma_L V_s(t - \frac{1}{v}(2nl + 2l - z))] & (n \geq 3) \end{aligned}$$

Choosing the observation position at  $z=0$ , the above expansion reduces to

$$\begin{aligned} V_o(0,t) &= T [V_s(t) + \Gamma_L V_s(t - \frac{2l}{v})] & (n=0) \\ &+ T \Gamma, \Gamma_L [V_s(t - \frac{2l}{v}) + \Gamma_L V_s(t - \frac{4l}{v})] & (n=1) \\ &+ T (\Gamma, \Gamma_L)^2 [V_s(t - \frac{4l}{v}) + \Gamma_L V_s(t - \frac{6l}{v})] & (n=2) \\ &+ T \sum_{n=3}^{\infty} (\Gamma, \Gamma_L)^n [V_s(t - \frac{2nl}{v}) + \Gamma_L V_s(t - \frac{2l(n+1)}{v})] & (n \geq 3) \end{aligned}$$

To simulate the TDR, the above expression needs to be considered for the  $n=0$  case only. This leads to

$$V_o(0,t) = TV_s(t) [1 + \Gamma_L] \quad (3.1.14)$$

### 3.2 Frequency-domain Analysis

An expression of the same form as Eq. (3.1.14) can be obtained for  $V_o(t)$  by using s-parameter analysis. This analysis begins by first recalling that

$$\begin{aligned}S_{11} &= \frac{b_1}{a_1} \\ a_1 &= \frac{V_{i1}}{\sqrt{Z_o}} \\ b_1 &= \frac{V_{r1}}{\sqrt{Z_o}}\end{aligned}$$

The observed voltage  $V_o$  as shown in Figure 11 is given by

$$\begin{aligned}V_o(\omega) &= \sqrt{Z_o} [a_1 + b_1] \\ &= \sqrt{Z_o} [a_1 + a_1 S_{11}(\omega)] \\ &= \sqrt{Z_o} a_1 [1 + S_{11}(\omega)] \\ &= \sqrt{Z_o} \frac{V_{i1}}{\sqrt{Z_o}} [1 + S_{11}(\omega)]\end{aligned}$$

$$V_o(\omega) = \frac{V_s(\omega)}{2} [1 + S_{11}(\omega)]$$

This implies that

$$V_o(t) = \mathbf{F}^{-1} \left\{ \frac{V_s(\omega)}{2} [1 + S_{11}(\omega)] \right\} \quad (3.2.1)$$

where  $\mathbf{F}^{-1}$  and  $V_s(\omega)$  denote the inverse Fourier transform operator and the Fourier transform of the excitation source, respectively.

## CHAPTER 4

### IMPLEMENTATION AND PERFORMANCE OF THE S-PARAMETER TDR

Equation (3.2.1) shows that in order to recover the observed voltage  $V_o(t)$ , both the Fourier transform  $V_i(\omega)$  of the excitation source  $V_i(t)$  and the measured values of  $S_{11}(\omega)$  of the DUT are needed. This makes it possible to observe the response of the DUT to any desired excitation source - as long as the source's Fourier transform can be derived. This allows the response of the DUT to be observed as the rise time of the excitation source is varied. It becomes possible then to observe how the DUT degrades as the system rise time is decreased. This is a significant advantage over conventional TDR techniques. Another advantage is the manner in which the measured values of  $S_{11}(\omega)$  are used. These measurements could have been taken by another network analyzer or retrieved from other data bases. The response of the represented DUT could then be predicted as a function of the excitation source, without having to make additional measurements.

Before implementing the above solution (Eq. (3.2.1)), the effects of system rise time, the frequency range of equipment, and the controller's processing speed must all be taken into account.

#### 4.1 System Rise Time

The system rise time  $t_r$  plays a major role in determining the resolution of physical discontinuities and also sets the frequency limits at which the system can make measurements. For example, if the distance from the source to the discontinuity is  $d_1$ , the elapsed time between generated and reflected

pulses is  $t_1$ , and the propagation velocity is  $v_p$ , then

$$d_1 = \frac{v_p}{t_1}$$

Likewise, the distance  $d_2$  between two discontinuities is given by

$$d_2 = \frac{v_p}{2}(t_1 - t_2)$$

Since it is impossible to distinguish between pulses when  $t_1 - t_2 < t_r$ , the minimum distinguishable distance,  $d$ , between two pulses is

$$d = \frac{v_p t_r}{4}$$

For example, a system with a 21-nanosecond rise time will make 2.57 meter resolutions. Discontinuities smaller than 2.57 meters will not be seen. For a 40-picosecond rise time, resolutions down to 3 millimeters can be made. The 3-dB frequency  $f_b$  that can be measured by the system is determined by

$$f_b = \frac{0.35}{t_r}$$

For the system with  $t_r = 21$  nanoseconds, the 3-dB frequency is only 16.6 MHz, while that with a 40-picosecond rise time is 8.75 GHz.

#### 4.2 Frequency Range of Equipment

Most network analyzers available for microwave applications have a frequency range of 0.5 to 18 GHz, which means that, in general,  $s$ -parameters cannot be measured below 0.5 GHz. Since Eq. (3.2.1) uses measured values of  $S_{11}$  at all frequencies, it will definitely affect how the TDR is implemented. Occasionally the test set can be forced to make measurements below 500 MHz without the network analyzer and the harmonic converter losing phase lock. This can successfully be accomplished with frequencies as low as 50 MHz.

For frequencies below 50 MHz (dc to 50 MHz), measured values for  $S_{11}$  must be extrapolated. In this thesis, values for  $S_{11}$  below 50 MHz were approximated by the measured value at 50 MHz, i.e.,

$$S_{11}(\omega) = S_{11}(2\pi f) \text{ for } 0 < \omega < 2\pi f; f = 50 \text{ MHz}$$

Another pertinent consideration is the interrelation between frequency range, pulse width, number of samples needed, and the length of transmission line that will be used when making measurements. In order to measure the DUT with a transmission line that is twice as long, the pulse width must be doubled. This will allow enough time for the reflected pulse to be intercepted before the second pulse is launched. To retain the same degree of "distinguishability," the number of samples must be doubled by halving the frequency steps at which samples will be taken. If the sampling distance was decreased, then the maximum sampling frequency must increase. Not taking enough samples means not acquiring enough data to effectively recover the true response of the DUT and could manifest itself by responses which appear to decrease in level. Some rise-time degradation may also show up. Hence, caution must be exercised when interpreting the  $V_{in}(t)$  values from Eq. (3.2.1).

#### 4.3 Processing Speed

As discussed above, changing the line length or trying to increase the resolution will affect the number of samples required. As the number of samples increases, more memory and more time are needed for processing the information. The speed of the FFT routine becomes very important when a large number of samples are used. This implementation utilized a radix-2 FFT algorithm that required  $2^n$  number of samples,  $n=2,3,\dots,10$  [11]. If only 300 sam-

ples were required for a particular resolution, then 512 measurements had to be made in order to satisfy the FFT routine.

#### 4.4 S-parameter TDR Performance

When making measurements, a regular trapezoid was used to model the excitation source  $V_i(t)$ . Pertinent quantities were defined as shown in Figure 12. In this way, the rise time,  $t_r$ , and the pulse duration,  $P_w$ , could be changed as desired. The analytic expression for the Fourier transformed source  $V_i(\omega)$

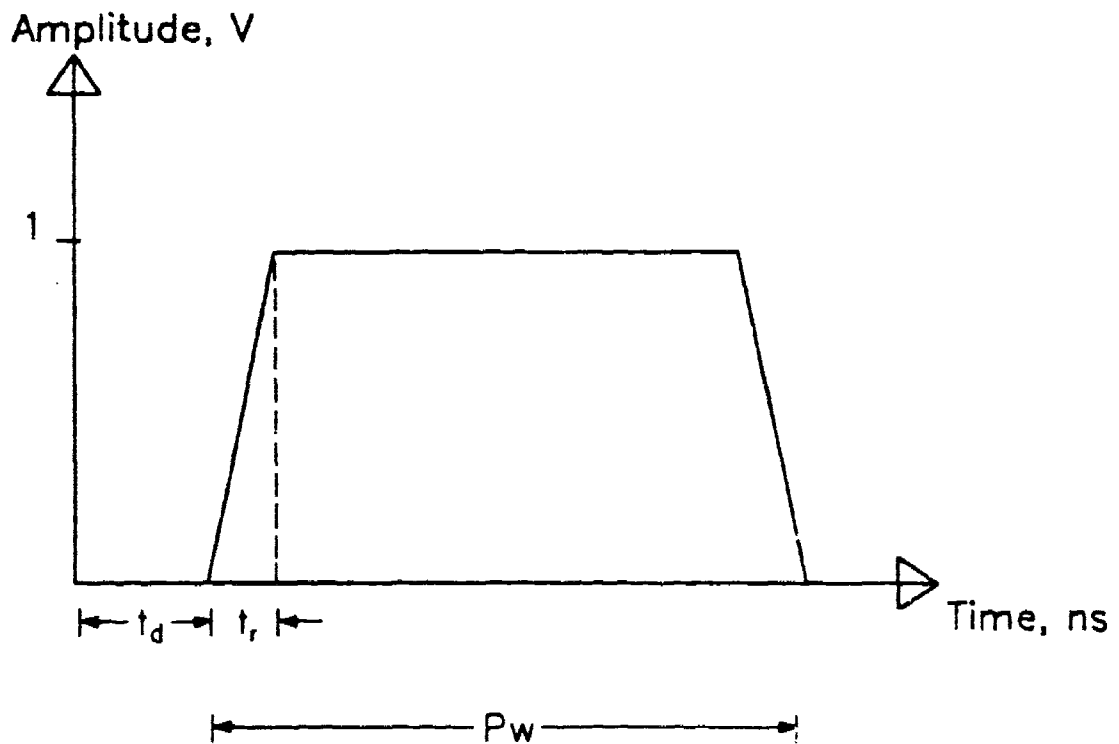


Figure 12. Input Excitation Pulse Used in the S-parameter TDR Simulation.

was then derived in terms of  $t_r$ ,  $t_d$ , and  $P_w$  as required in Eq. (3.2.1).

In the results shown later (Figures 13 through 15), typically there appears first a time delay  $t_d$ , which was artificially introduced so that the response would not appear flush against the left edge of the plots. This does not affect the true response of the DUT. After the time delay  $t_d$ , the rising edge of the pulse is seen, followed by a matched 50-ohm line or connector used as a 50-ohm reference. The 50-ohm reference corresponds to a level of 0.500 V, since the default amplitude of the excitation source was 1.000 V. Levels of the response appearing above this reference indicate that the input impedance of the DUT is greater than 50 ohms, while levels below indicate an input impedance between 0 and 50 ohms. The maximum ranges of the response correspond to open and short terminations, with the response doubling to 1.000 V and dropping to 0.000 V, respectively.

Figure 13 shows the time-domain response when the reference 50-ohm line was terminated in an open circuit. Note the delay  $t_d$  (0.5 ns) followed by the 50-ohm reference line at 0.500 V and then the doubling to 1.000 V due to the open termination. The level changed again at 3.5 ns when the falling edge of the excitation pulse occurred. In Figure 14, the response simulated that of a matched load terminating the 50-ohm reference line. After the time delay  $t_d$ , the level remained at 0.500 V for the entire pulse duration, then dropped when the falling edge of the pulse occurred. Figure 15 shows the response when the 50-ohm reference line was terminated in a short. Again, the time delay  $t_d$  is followed by the 50-ohm reference line. At the end of the line, the level dropped back to 0.000 V and then changed again when the pulse ended at 35 ns.

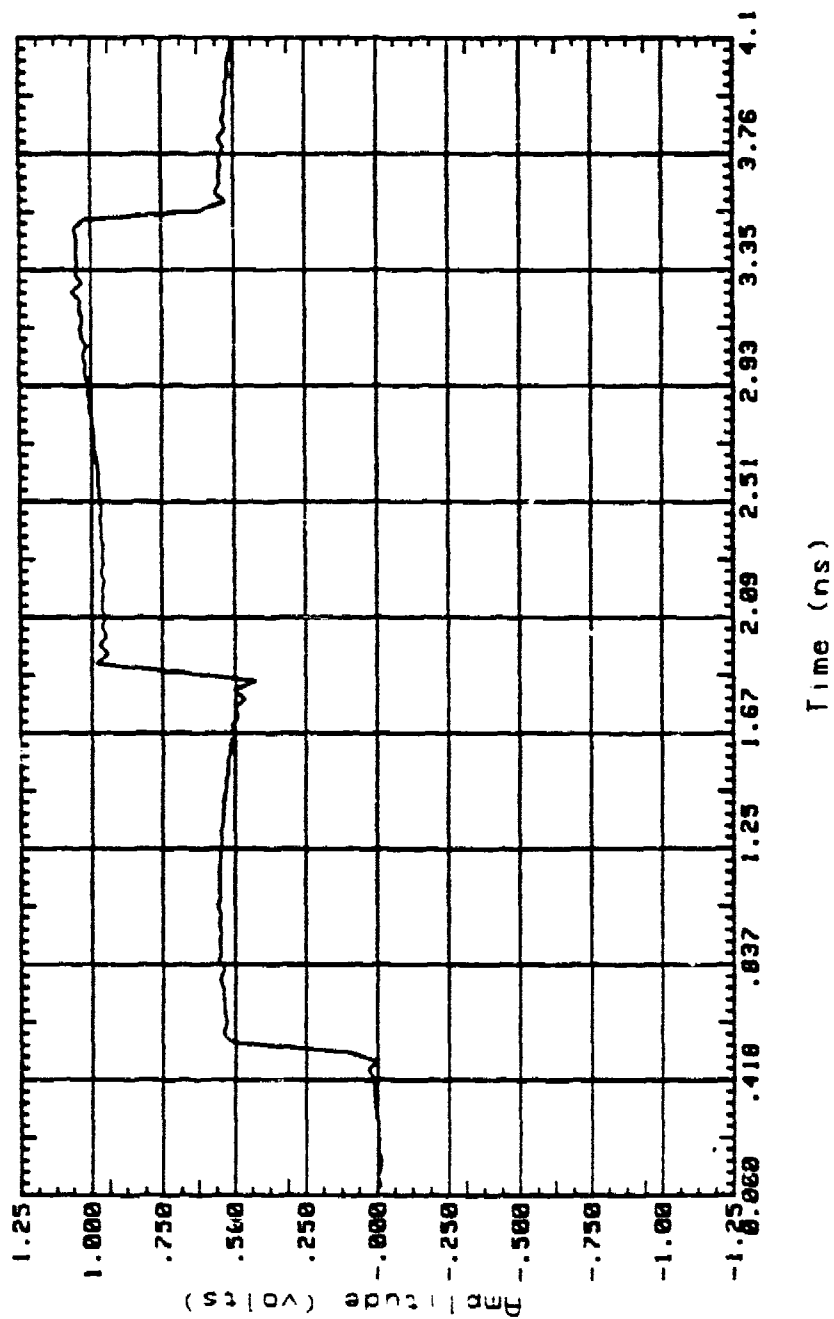


Figure 13. Pulse Response of an Open-circuit Termination.

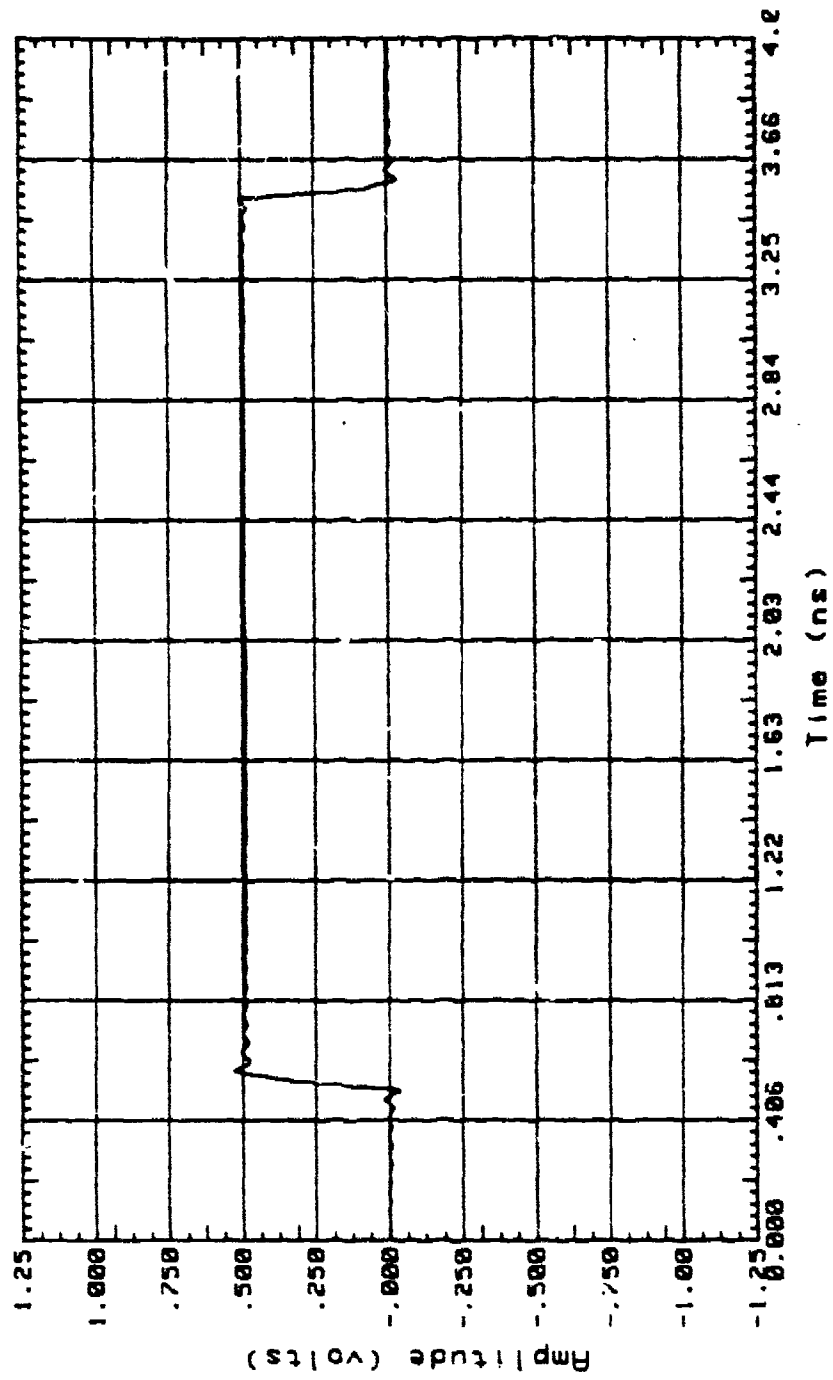


Figure 14. Pulse Response of a Matched 50-ohm Termination.

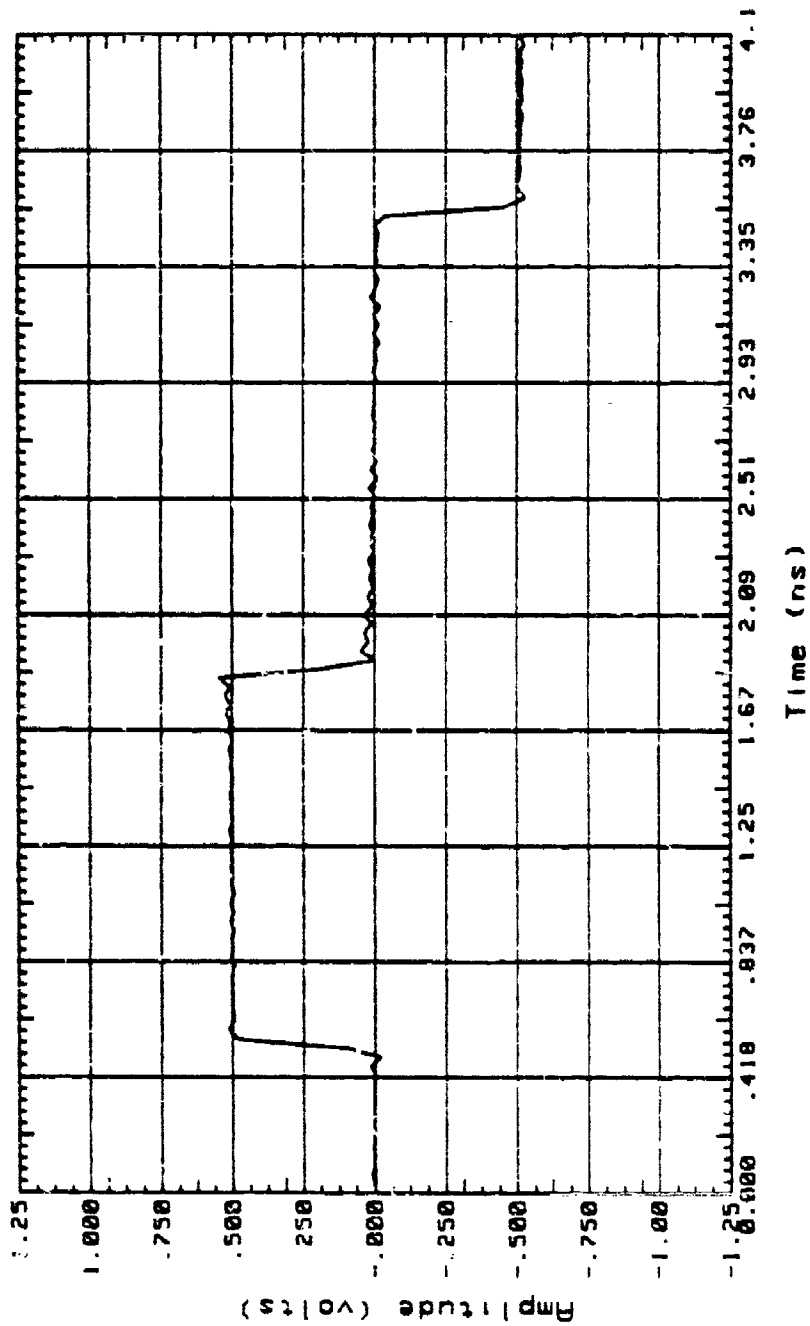


Figure 15. Pulse Response of a Short-circuit Termination.

The above three responses very accurately simulate those of conventional TDRs for open, matched, and short terminations. They are exactly what is expected from conventional TDRs. As a further demonstration of this accuracy, Figures 16 and 17 show the responses of two different DUTs as measured by the *s*-parameter TDR and by a conventional TDR which used a pulse generating scope. The response of the conventional TDR is displayed as an inset superposed on that of the *s*-parameter TDR simulation. Figure 16 is the response of a microstrip line, while Figure 17 is that of an AMP connector. The general shape of the responses shows excellent agreement and the *s*-parameter simulation provided better resolution than the conventional TDR. This advantage is discussed further in the next section.

#### 4.5 Advantages of the S-parameter TDR

As mentioned earlier, the TDR utilizing *s*-parameters has some significant advantages over conventional TDRs. The most salient is the versatility it allows in selecting a source. Conventional TDRs offer a single source with a fixed rise time. With the *s*-parameter implementation, any source can be used to check the response of the DUT. Often, it is of primary interest to determine the point at which significant degradation in rise time occurs. To determine this point, the rise-time variable  $t_r$  in the measurement program can be varied while observing the response,  $V_o$ , of the DUT. It is also very simple to access the measurement program written for this implementation and change the pulse width,  $P_w$ , as desired.

Another advantage is the increased resolution this implementation provides as seen in Figure 16, which shows the response of a microstrip line. The

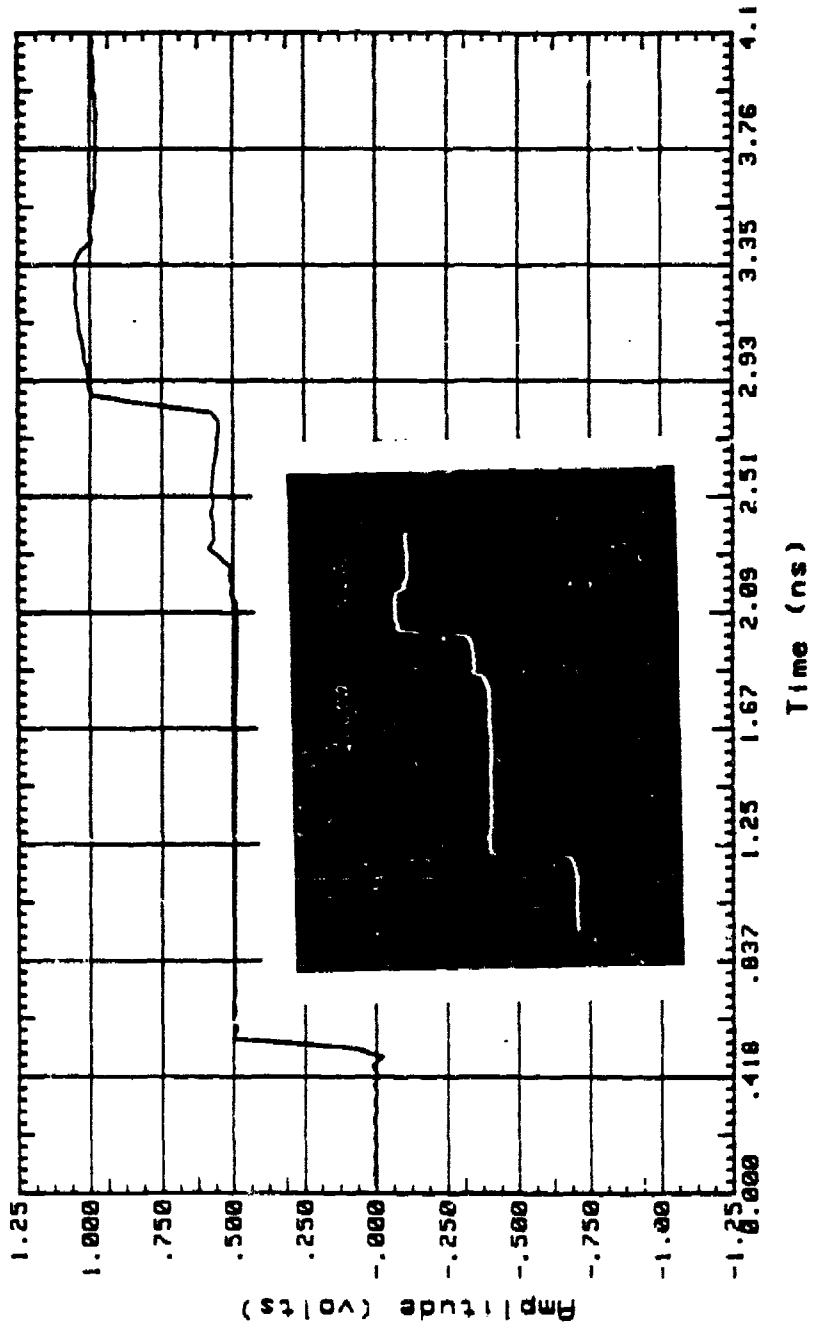


Figure 16. Pulse Response of a Microstrip Line.

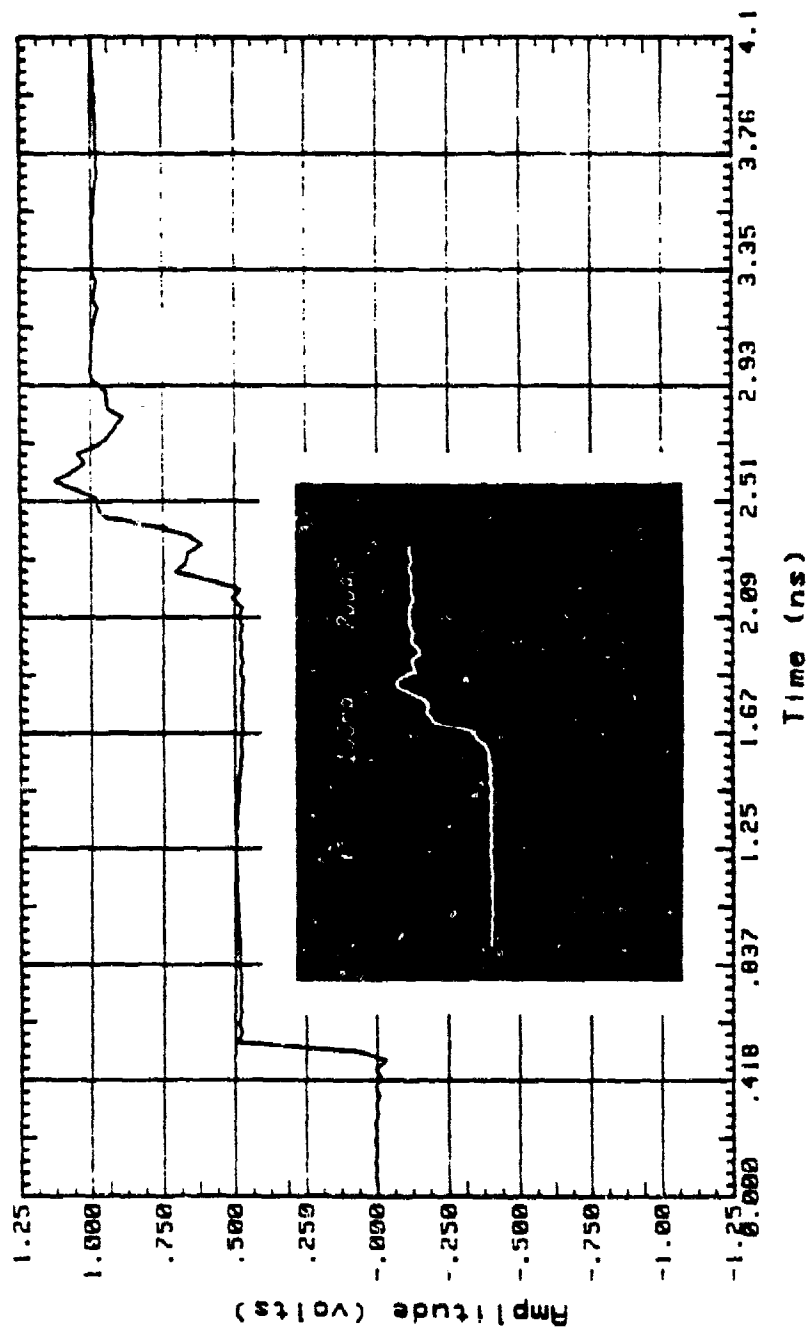


Figure 17. Pulse Response of an AMP Connector.

loss due to the microstrip line is noticeable when viewed on the  $s$ -parameter TDR. This information is lost on the conventional TDR (inset). The increased resolution of the  $s$ -parameter TDR is seen again in Figure 17, which shows the response of an AMP connector. The conventional TDR used a scope with a rise time of about 40 picoseconds (inset). Forty picosecond rise-time scopes are among the fastest presently available and provide a 3-dB frequency of about 9 GHz. With a 3-dB frequency of only 9 GHz, the conventional TDR loses much high frequency information about small discontinuities. The response of the same connector using the  $s$ -parameter technique is shown in the background of the same figure. Note that the connector is much more visible now. The  $s$ -parameter TDR was able to retain much of the information at high frequencies because a shorter rise-time pulse was used. In the  $s$ -parameter TDR, it is clearly seen where the connector begins. Not so for the inset. The  $s$ -parameter TDR simulation was not constrained by the 3-dB frequency  $f_3 = 0.35/t_r$ , since the rise time  $t_r$  could be made as small as desired.

Perhaps the most significant advantage of this technique, however, is the ease with which the data can be processed. The information obtained from a conventional TDR is not readily accessible for processing. The  $s$ -parameter technique has no such constraint. As a matter of fact, it was this particular feature that was utilized in solving the "de-embedding" problem.

## CHAPTER 5

### THE DE-EMBEDDING PROBLEM AND SOLUTION

Time-domain reflectometry has many applications. Oliver [1] utilized it for locating discontinuities in transmission lines. Luce et al. [12] were able to determine loss and dispersion in microstrip lines and coaxial cables. Nicholson et al. [3] described how it may be used to determine *s*-parameters, constitutive parameters of microwave materials, driving-point impedances and transfer functions of microwave antennas, and frequency-domain scattering parameters of conducting surfaces in free space. In this thesis, the TDR application was restricted to removing unwanted distortion which resulted from connectors during the measurement process.

As mentioned in the introduction, the TDR technique was developed to solve the de-embedding problem. The objective was to remove the effects of any intervening connections between the measuring set and the DUT (Figure 18). This was motivated by a desire to "see" the DUT alone and not the DUT/connector composite. As evidenced by Figure 19 (p. 44), which is the time-domain response of the DUT, (C1OP), the TDR technique indicated where the connector began. It was not so easy to determine where it ended and where the DUT actually started.

Before the effects of the connector can be gated out, its boundaries must be determined. Marking the beginning of the connector was a relatively easy task as explained below. To mark where it ended, the connector was terminated with a matched 50-ohm load. Theoretically, this should show up as a sharp transition back to the 50-ohm reference, thus precisely determining

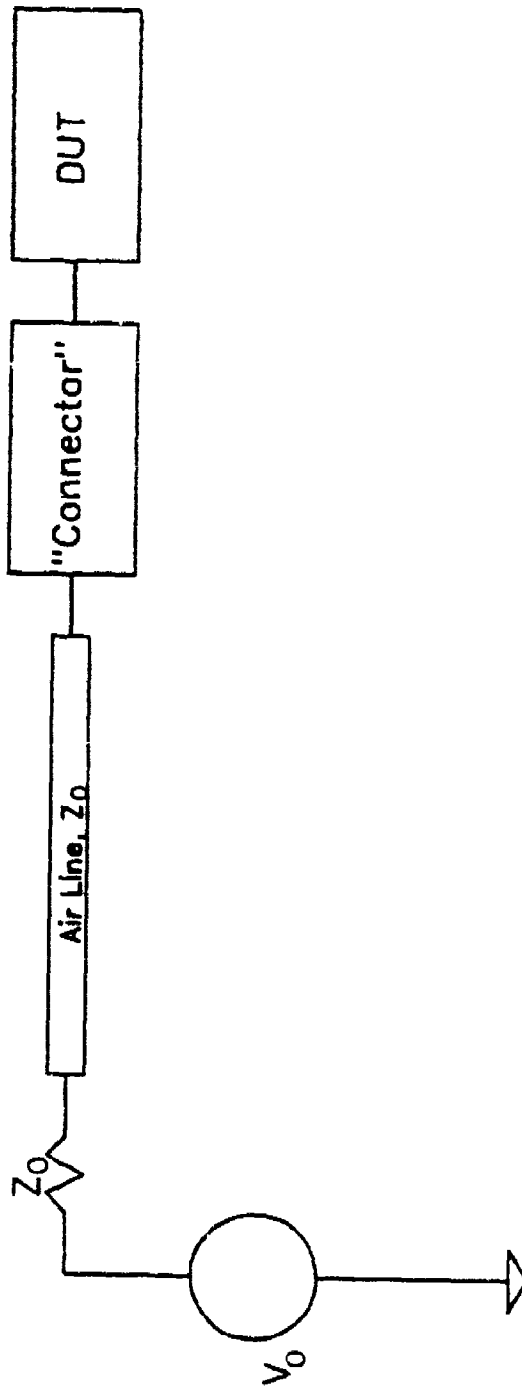


Figure 18. Schematic Representation Showing the "Connector" To Be De-embedded.

where the connector ended and where the DUT began.

While the above theory sounded reasonable, it was difficult to implement. The difficulty stemmed from the response's slow deviation from the 50-ohm reference. If the response showed sharp deviations from the 50-ohm reference, it would be simple to mark where the connector began and ended and quite easy to gate it out. Since this was not the case, a scheme was developed to mark the terminals of the connector. In this scheme, levels of the response were compared to those of the 50-ohm reference (0.500 V). A tolerance  $\delta$  was chosen, and data points were evaluated to determine which ones fell within the range  $0.500V \pm \delta$ . When three successive points fell within the tolerance range, the first one was used as a marker. To mark the beginning of the connector, the first set of three data points falling within the tolerance range was used; the second set was used to mark the end of the connector. Three successive data points were selected as the criteria by reasoning that power spikes and surges will most likely perturb at most two data points. It was also desirable to avoid false markings in case the connector itself had a response with multiple 50-ohm crossings.

The above scheme was utilized in extracting the effects of the connector as demonstrated in Figures 19 through 21. Figure 19 shows the unprocessed time-domain response of a DUT (CIOP) terminated in an open circuit. Preceding the DUT was a connector which clearly showed up as the first significant deviation from the 50-ohm reference. Figure 20 shows the response when the DUT was replaced by a matched 50-ohm load. Note here that the response did transition back to the 50-ohm reference line, but did so very slowly. This gradual transition meant that a judgement had to be made as to where the connector actually ended. The tolerance testing criterion was applied and

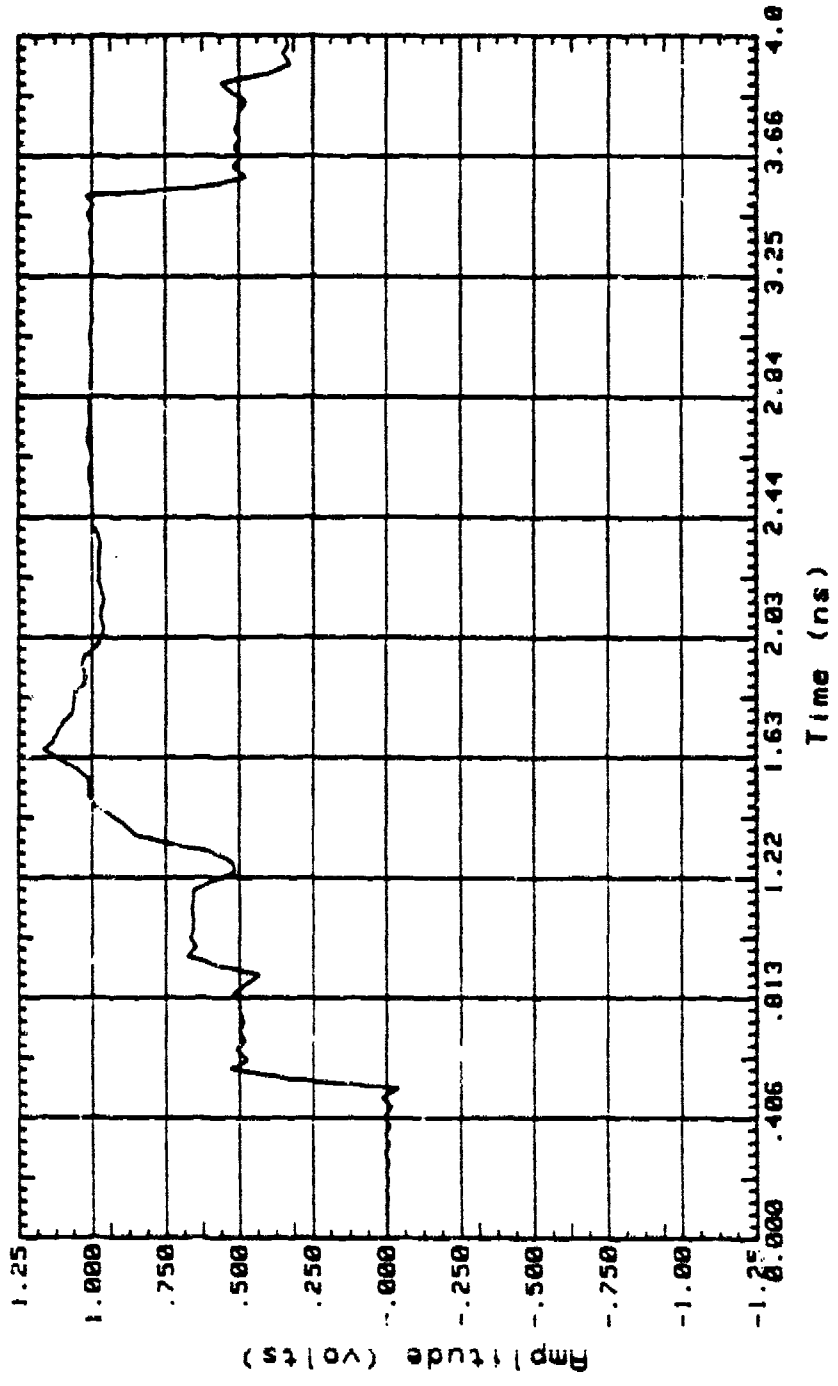


Figure 19. Pulse Response of the DUT, C10P.

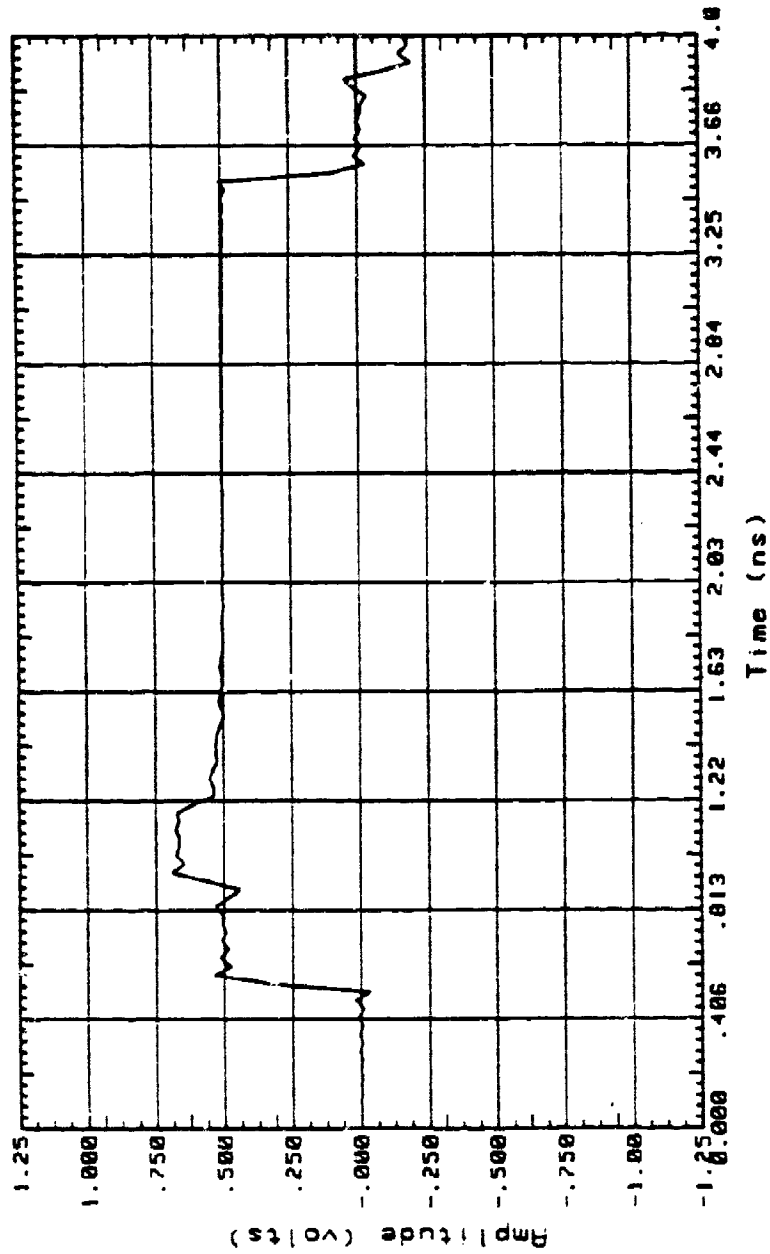


Figure 20. Pulse Response When DUT Was Replaced by a Matched Load.

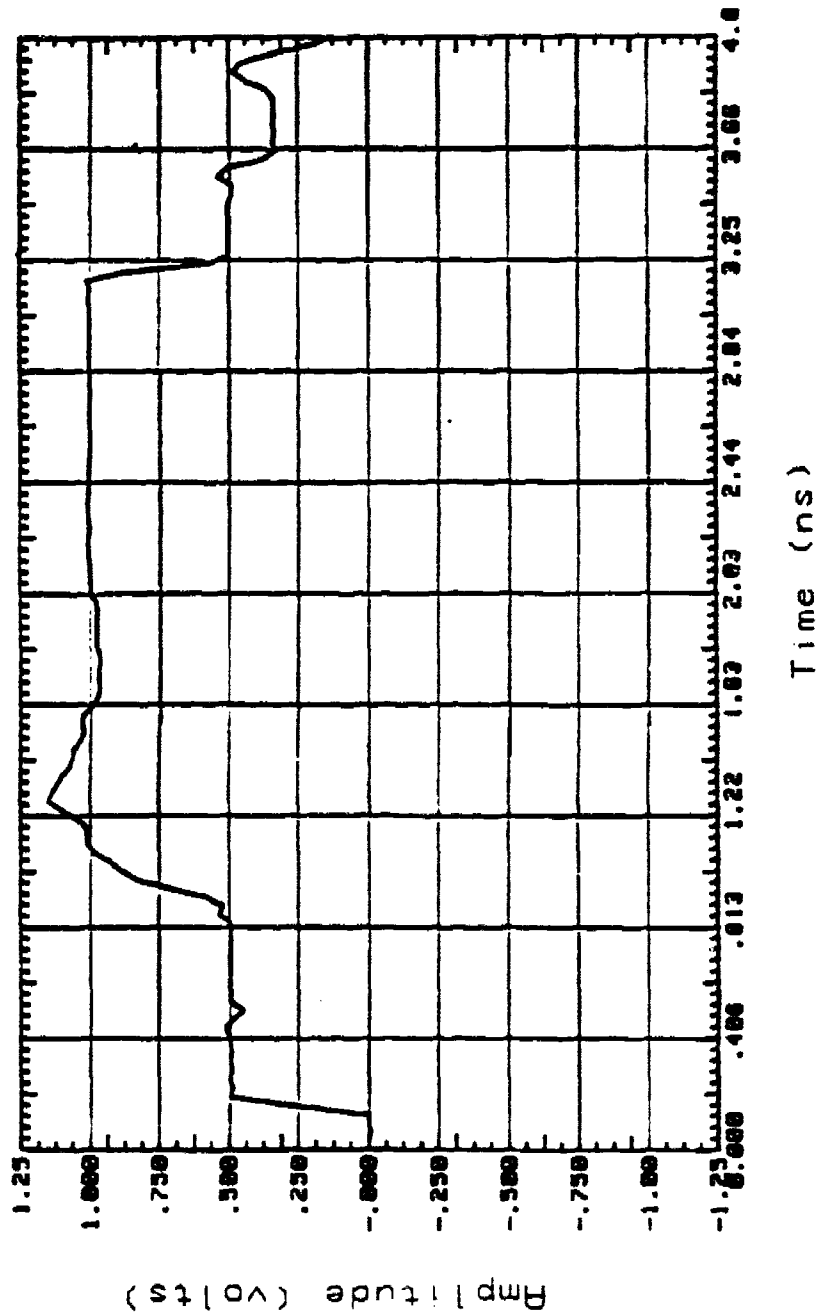


Figure 21. "Connector-free" Pulse Response of DUT.

eventually the most probable end point was marked. Equipped with both the beginning and end terminals of the connector, it was gated out. The resulting time-domain waveform then represented the response of the DUT alone as shown in Figure 21.

## CHAPTER 6

### CONCLUSIONS AND FUTURE WORK

This study utilized measured values of the s-parameter  $S_{11}$  to develop a time-domain reflectometer. The s-parameter TDR performed better than conventional scope type TDRs because the rise time of its excitation source can be made arbitrarily small. This feature also permitted examination of the response of a DUT as a function of rise time. It can potentially be used to determine the point at which significant rise-time degradation occurs.

The s-parameter TDR was applied successfully to the de-embedding problem. The effects of the intervening connector between the measuring set and a one port DUT were effectively removed. The scheme by which the de-embedding was accomplished was not an optimum one since it did not precisely mark the exact terminals of the connector. Some work is needed to determine more accurately where the connector begins and ends so that gating it out can produce a response that is as "connector free" as possible. Work is also needed to determine the effects of truncation when using the FFT routine. This was not investigated. Finally, work is needed to transform the "connector-free" time-domain response to the frequency-domain, enabling design engineers to further analyze their DUTs.

## LIST OF REFERENCES

- [1] B. M. Oliver, "Time Domain Reflectometry," *Hewlett Packard Journal*, vol. 15, February 1964.
- [2] A. S. Farber and C. W. Ho, "Wide-band Network Characterization by Fourier Transformation of Time-domain Measurement," *IEEE Journal of Solid State Circuits*, vol. SC-4, no. 4, pp. 231-235, August 1969.
- [3] A. M. Nicholson, C. L. Bennett, D. Lamensdorf and L. Susman, "Applications of Time-domain Metrology to the Automation of Broad Band Microwave Measurements," *IEEE Transactions on Microwave Theory and Techniques*, MTT-20, pp. 3-9, January 1972.
- [4] R. F. Bauer and P. Penfield, Jr., "De-embedding and Unterminating," *IEEE Transactions on Microwave Theory and Techniques*, MTT-20, pp. 282-288, March 1978.
- [5] H. W. Loeb and P. J. Ward, "The Use of Time-domain Techniques for Microwave Transistor S-parameter Measurements," *IEEE Transactions on Instrumentation and Measurement*, IM-26, pp. 383-388, December 1977.
- [6] K. Kurokawa, "Power Waves and the Scattering Matrix," *IEEE Transactions on Microwave Theory and Techniques*, MTT-13, pp. 194-202, March 1965.
- [7] "S-parameter Techniques for Faster, More Accurate Network Design," *Hewlett-Packard Application Note AN 95-1*.
- [8] "Basic Measurements," *Hewlett-Packard Manual for the HP-8510 Network Analyzer*, pp. 69-119, May 1983.

- [9] S. J. Mason, "Feedback Theory - Some Properties of Signal Flow Graphs," *Proceedings of IRE*, vol. 41, no. 9, pp. 1144-1156, September 1953.
- [10] S. J. Mason, "Further Properties of Signal Flow Graphs," *Proceedings of IRE*, vol. 44, no. 7, pp. 920-926, July 1956.
- [11] E. O. Brigham, *The Fast Fourier Transform*. Englewood Cliffs: Prentice Hall, 1974.
- [12] D. A. Luce, H. M. Cronson, and P. G. Mitchell, "Time-Domain Measurements of Loss and Dispersion," *IEEE Transactions on Microwave Theory and Techniques*, MTT-24, pp. 50-54, January 1976.